



PVA-CNCs composite electrospun nanofibers for poly(lactic acid) polymer reinforcement

J. Elliott Sanders¹ · Yousoo Han¹ · Todd S. Rushing² · Evan K. Wujcik³ · Douglas J. Gardner¹

Received: 20 July 2023 / Revised: 6 May 2024 / Accepted: 8 August 2024
© The Author(s), under exclusive licence to Springer Nature Switzerland AG 2024

Abstract

In this study, poly(vinyl alcohol) (PVA) in a water solution was mixed with CNC suspensions in 4:1 and 3:2 weight ratios (w/w) and electrospun (ES) into aligned composite fiber mats. The electrospun mats were mechanically cut into high aspect ratio nanofibers (PVA:CNC-nf) and used as reinforcement in melt compounded thermoplastic poly(lactic acid) (PLA). A control PLA composite, containing neat electrospun PVA fibers (PVA-nf) and electrospayed CNC nanoparticles (CNC-np), was produced for each composite fiber ratio. The electrospun nanofibers (ESNFs) were observed to maintain their morphology without exhibiting agglomeration or void formation in the PLA matrix. Composites containing 15 wt.% 4:1-nf improved tensile strength and stiffness of the PLA by 21% and 30%, while reducing strain at break by 7%, and increased PLA impact strength by 54%. In comparison, the 12 wt.% neat PVA-nf improved the PLA tensile strength and stiffness by 19% and 8%, respectively, while increasing tensile strain at break by 24% and impact strength by 30%. Toughness analysis indicated that the neat PVA-nf improved PLA specific tensile strength, despite the 4:1-nf absorbing more impact energy. Flexural strength improved slightly with the 3:2-nf, but flexural stiffness generally decreased, apart from 15% and 7.5% filled 4:1-nf and 3:2-nf filled PLA composites. Mechanical improvements were attributed to the electrospun reinforcement fibers' nanometer dimensions and interfacial compatibility, based on by the shift to bound hydroxyl groups detected in the Fourier transform infrared spectroscopy (FTIR) analysis for the PLA composites.

Keywords Electrospinning · Cellulose · Poly(vinyl alcohol) · Composite nanofiber · Mechanical reinforcement · Poly(lactic acid) · Cellulose nanocrystals · PLA composite · Nanofiber

1 Introduction

1.1 Bio-based polymers and sustainability

Sustainable bio-based polymers have gained significant interest since the early 2000s, and the scientific literature surrounding their use, improvement, and applications has increased. A meta-analysis of the last 20 years reported that 1874 research papers were published on bio-based plastics and that over half of those papers were published

between 2018 and 2021 (approx. 20% in 2021), demonstrating a growing interest in the use of sustainable plastics [1]. According to the same study, the bio-based polymers that garnered the most research interest are poly(lactic acid), poly(hydroxyalkanoate), poly(hydroxy butyrate), and poly(butylene succinate). Lastly, the study specified that the key objective related to the use of poly(lactic acid) (PLA) was its mechanical properties, where food packaging generated the largest demand in interest.

PLA is a polar thermoplastic making it compatible with natural fillers, and it possesses high tensile strength and stiffness, depending on the grade. However, it exhibits a slow crystallization rate, poor thermal resistance, and deformation at temperatures above 50 °C [2]. These drawbacks, along with its higher cost compared to conventional plastics, hinder its use in semi-structural and structural applications. Unlike its fossil-fuel-derived competitors, namely biaxially oriented poly(propylene) (BOPP) and general-purpose poly(styrene) (GPPS), PLA is produced from renewable

✉ J. Elliott Sanders
jsande80@maine.edu

¹ Advanced Structures and Composites Center (ASCC),
University of Maine, Orono, ME, USA

² US Army Engineer Research and Development Center
(ERDC), Vicksburg, MS, USA

³ Materials Engineering and Nanosensor (MEAN) Laboratory,
University of Maine, Orono, ME, USA

sources like corn syrup or sugar beet pulp (SBP). A techno-economic analysis reported that with SBP-production methods, the cost of PLA would reach approximately \$1.14/kg with the sales of a pectin-rich extract, a byproduct of PLA production, reaching \$3–4/kg [3]. In comparison, BOPP and GPPS cost \$1.4 and \$1.72/kg, respectively.

1.2 Cellulosic nanomaterials

Cellulose nanomaterials (CNs) are widely abundant and naturally occurring around the world. These materials offer high specific strength and stiffness, thermal stability, and chemical functionalization through the abundantly available surface hydroxyl groups (-OH) [4]. However, CNs often require additional treatment to improve hydrophobic matrix compatibility, reduce hydrophilicity, and increase thermal resistance [5]. Cellulose containing only the crystalline components is commonly used for composite reinforcement because of the high axial strength (1.6–6.4 GPa) and stiffness (57–180 GPa) [5].

Cellulose nanocrystals (CNCs) are derived by alkaline or acid hydrolysis from a variety of sources with varying efficiencies [6], and, in suspension, CNCs exhibit two dimensions within the nanoscale. However, after dehydration or compounding, CNCs increase in size by agglomeration, especially with increased weight concentration [7, 8]. This particle size increase occurs when liquid media is removed from the suspension by one of many drying methods [9], where self-interactions are promoted by a multitude of mechanisms [10], including hydrogen bonding [11]. Agglomeration is prevented by surface functionalization or sizing of CNCs, typically by acetylation or with a silane coupling agent for inorganic compatibility, that can increase hydrophobicity or promote covalent bonding for improved matrix interactions [12].

Natural fillers like CNCs work to improve the mechanical properties, but the strength and stiffness are dependent on the filler length. When a nanocellulose filler is compounded in a thermoplastic matrix, a homogeneous distribution of the filler, with good interfacial compatibility, improves the composite properties including strength and stiffness at low (> 1%) filler content [13, 14], but typically at the disadvantage of elongation at break, toughness, and impact strength properties [13]. Improved fiber dispersion and surface interaction dictate what amount of surface area interacts with and improves the properties of the compounded polymer matrix.

1.3 Poly(vinyl alcohol) and cellulose nanocrystals

Poly(vinyl alcohol) (PVA) is a vinyl polymer connected by carbon–carbon bonds with -OH groups and is produced from polyvinyl acetate after hydrolysis, which can be sustainably produced from ethanol [15]. PVA is biodegradable by

fungal or bacterial organisms in aerobic or anaerobic environments [16]. PVA is water soluble below the boiling point of water at sea level and atmospheric pressure (100 °C), is non-toxic, and offers biocompatibility and ductility [16, 17]. The hydroxyl functionality presents a major advantage in interfacial compatibility when compounded with CNCs, and these composites can be processed into hydrogels [18] and films [19], wet spun into single fibers [20], and electrospun (ES) into nanofiber mats [21, 22].

The tensile strength and stiffness properties of the various composite CNC forms range from 0.1 to 1000 s of MPa in tensile strength and 0.0001 to 10 s GPa elastic modulus [23]. The composite PVA fiber morphology, especially ES nanofibers, is an attractive option for use as a mechanical reinforcement filler in thermoplastic PLA because of the polar compatibility, high specific tensile strength (100–1000 s MPa), and specific elastic modulus (10–100 s GPa). Furthermore, thermal degradation temperature (225–230 °C) [24] is within the melting range of PLA, especially when combined with CNCs that degrade around 317–330 °C [25]. The utilization of ES composites can address the reduction in agglomeration of CNCs by encapsulation within PVA and the interfacial compatibility of PVA in PLA with respect to surface energy [26, 27].

Electrospinning is a technique that manipulates liquid media with electric fields and low amounts of current through an air gap. The ES method gained popularity in the early 2000s using a single capillary metallic needle (SNE) connected to a high voltage electric potential (+/–), which generates an electric field. The solution is mechanically pumped by a syringe and propelled by the high voltage to produce nanoscale fibers that accumulate into a random nonwoven mat. Furthermore, a rotating collector can be used to align the fibers [28]. Production with a single needle range from 0.01–0.1 g/h of spun nanofibers, but with advancements in free surface [29] and shear-aided [30] electrospinning, the productivity of spun fibers can increase to 1–10 s g/h, depending on the dissolved polymer viscosity and conductivity. This increased productivity can also occur without reducing the continuous fiber quality or increasing the fiber diameter [31].

Over the past two decades, the interest in ES has increased from hundreds of publications in the early 2000s to thousands a year in the past 5 years, with about one-third of those studies relating to composites [32]. Electrospun fibers exhibit an internal alignment of polymer chains from the elongation process that improve strength, elongation and toughness properties, promoting their use as fiber reinforcement in polymer resins [33]. Various composites have been produced by incorporating organic and/or inorganic fillers into the dissolved polymer solutions to spin composite fibers into mats, forming hybrid composite mats by co-spinning multiple polymer solutions, utilizing

the neat polymer or composite mats as continuous reinforcement in solvent casted films and epoxy resins, and by compounding continuous fiber mats between thermoplastic sheets by thermal compression molding [34–36].

1.4 Research objective

Recent literature reviews have expressed a need for further investigation into short fiber reinforcement in polymer resins [32, 37]. Few processes offer both an ability of surface modification and production of nanofibers with the option of controlling the fiber lengths as a melt compounding additive. Producing fibers with controlled aspect ratios allow for further analysis of the critical aspect ratio and lengths associated with optimization of the composite stiffness [23]. Additionally, natural fiber PLA composites are brittle and often lack toughness once reinforced. Investigation into ductility and impact strength using fiber reinforcement presents an opportunity to broaden the applications of PLA. Therefore, this research is focused on using well known and compatible components like PVA and CNCs, implementing the facile production of composite ESNFs by electrospinning and evaluating them as cut fiber reinforcement in a thermoplastic (PLA) matrix within the industrially scalable convention of melt compounding. The work done in this study investigated the challenges of producing nanometer diameter composite fibers from mixing PVA solution and CNC suspension, the processing steps related to producing discontinuous fibers from nonwoven mats, compounding the fibers, and characterization of the composite material and mechanical properties.

2 Materials and methods

2.1 Electrospinning solution

Electrospinning solutions were prepared by dissolving a 99% hydrolyzed PVA with a Mw of 130,000 g/mol that was purchased from Sigma-Aldrich (St. Louis, MO, USA) in water and mixing it with a 10.3 wt.% CNC suspension produced by the Forest Products Laboratory (FPL, Madison, WI, USA). Surface tension of the PVA and PVA/CNC mixtures was reduced by addition of 0.5% (v/v) of Triton X-100 with a Mw of 80,000 that was purchased from Sigma-Aldrich (St. Louis, MO, USA). Solution preparation is detailed in previous work [22]. The ESNFs processing conditions were selected with respect to consistency of fiber diameter and alignment, while maximizing CNCs wt.% content during electrospinning at the specified parameters listed in Table 1.

Table 1 Electrospinning and spraying settings used for production of composite filler by type

Filler type ID	Voltage kV	TCD cm	Feed rate $\mu\text{L}/\text{min}$	Needle length in	Collector speed m/s
4:1-nf	20 \pm 1	16–20	21	1–1.5	3.78
3:2-nf	20 \pm 1	16–20	21	1–1.5	3.78
PVA-nf	20 \pm 1	16–20	21	1–1.5	3.78
CNC-np	27	15	6	1–2	0

2.2 Sample preparation

The reinforcement fibers were first prepared by electrospinning PVA and CNC composite nanofibers in 4:1 (4:1-nf) and 3:2 (3:2-nf) ratios and PVA nanofibers as control reinforcement for the two types of composite nanofibers, at room temperature (24 ± 1 °C) and humidity (50 ± 10 , %). The CNCs, detailed in previous work [38], were electrospayed under the same environmental conditions, accumulated on a planar collector, removed by a straight edge, and collected in a beaker.

The ESNFs were prepared for compounding by first cutting 1–5-mm strips of the spun mat perpendicular to the alignment direction with an IDEAL 1071 (Krug & Prister GmbH & Co. KG, Balingen, Germany), 710-mm guillotine blade, and woven mat cutting board. Afterwards, the strips were cut along the orientation direction into squared mat sections. The sections were soaked for a minimum of 3 min in liquid nitrogen that was contained in a steel “Cryo-Cup” (Research Products International Corp, Mt. Prospect, IL USA) and plastic housing to increase the fiber stiffness prior to blending, at sub ambient temperatures, with a coffee grinder (Mr. Coffee: model#: IDS77RB; Cleveland, OH USA), which was equipped with a stainless-steel/plastic cup and twin steel blades for two 10-s periods. This process separated the fibers from their as spun state to produce fibrous bundles as shown in Fig. 1.

2.3 Thermoplastic compounding and specimen preparation

The sample identifiers (ID) are named by filler type. The IDs are differentiated by the ratio of PVA:CNC-nf as 4:1-nf and PVA:CNC2-nf as 3:2-nf. The PVA nanofibers, PVA-nf and PVA2-nf, correspond as references to the PVA wt.% content with respect to the two composite fillers. The weight percent (wt.%) of each fiber type is listed in Table 2 along with the ratio of PVA:CNC and wt.% of PLA matrix in the composite. The electrospayed CNC nanoparticles (CNC-np) were included as a reference for both composite nanofiber groups with equal CNC weight contents as composite ESNFs [38].

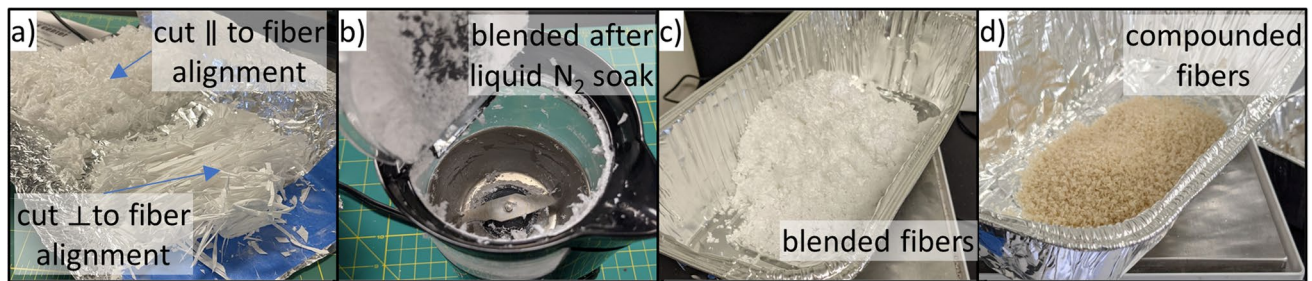


Fig. 1 Processing steps including **a** strips cut from the continuous fiber mat, **b** liquid nitrogen soaked and **c** blended fiber bundles, and **d** the melt compounded bundles in a PLA matrix

Table 2 Composition details for the studied materials

Filler type ID	Filler wt. %	Mix Ratio PVA:CNC	PLA wt. %
neat	0	0:0	100
4:1-nf	2.5	4:1	97.5
	5	4:1	95
	15	4:1	85
PVA-nf	2	1:0	98
	4	1:0	96
	12	1:0	88
CNC-np	0.5	0:1	99.5
	1	0:1	99
	3	0:1	97
3:2-nf	1.3	3:2	98.7
	2.6	3:2	96.7
	7.5	3:2	92.5
PVA2-nf	0.8	1:0	99.8
	1.6	1:0	97.4
	4.5	1:0	93.5

The fillers were conditioned at 60 °C for 4 h prior to melt compounding.

Thermal compounding was done in 100 g quantities using general grade 4043D Ingeo Biopolymer PLA pellets (Minnetonka, MN) in a batch mixer (C.W. Brabender Instruments Hackensack, NJ) at 180 °C for 3 min at 70 RPM. Fillers were then added and mixed for another 5 min. The contents were cooled at ambient conditions and reduced to ≤ 3 -mm pieces by a granulator (Hellweg MDS 120/150, Hackensack, NJ, USA).

2.4 Scanning electron microscopy (SEM)

Scanning electron micrographs were taken with a Zeiss NVision 40 (Oberkochen, Germany) electron microscope. Samples were observed under a 3 kV electron beam intensity and a 12 ± 1 mm working distance after sputter coating with a 4-nm-thick layer of gold palladium. Fracture surfaces of

the impact testing bars were observed at low magnification ($\times 50$) and high magnification ($\times 5.0$ k+).

2.5 Atomic force microscopy (AFM)

Thermoplastic composites were cut with an Ultra-AFM Diamond Knife 35° 3.0 mm knife into 1×2 mm area and 700-nm thick ribbons with a Leica EM UC6 (Leica Mikrosysteme GmbH, Vienna) for observation on the MFP3D (Oxford Instruments Oxon, UK) AFM. Images were collected with AC160TS-R3 probes with ~ 20 (nN/nm) spring constants. Alternating current (AC) mode produced images with a constant free air (1.5 V) amplitude to set point (0.5 V) ratio of 0.33.

2.6 Differential scanning calorimetry (DSC)

The composite melting temperatures were measured with a DSC 2500 (TA Instruments New Castle, DE USA) using T-zero aluminum pans and a heat-cool-heat cycle with an isothermal hold after heating and cooling, a ramp rate and temperature range of 5 min, 10 °C/min, and 20–200 °C, respectively. Sample measurements consisted of approximately 8 mg of sample and were repeated in triplicate.

2.7 Density

Specific gravity measurements were taken following D792-20 protocol at 23 °C.

2.8 Mechanical properties—tensile, flexural, and impact measurements

Tensile, flexural, and impact samples were injection molded using a Mini-Jector Model #50 (Miniature Plastic Molding, Solon, OH, USA) at 180 °C with an injection pressure of 17 MPa in accordance with ASTM D638-14 and D790-10. Tensile and flexural tests were conducted using a universal testing machine (Instron 5966) with a 10kN loadcell (Norwood, MA, USA) at 23 ± 2 °C and

relative humidity (RH) of $50 \pm 10\%$. Type I tensile specimens were tested at a 5 mm/min rate using a 50-mm gauge length and flexural specimens of $125 \times 12.7 \times 3.2$ -mm dimensions were tested with a 16:1 span to depth ratio at 1.4 mm/min. The flexural test specimens were used to measure impact resistance according to D256-10 on a Ceast pendulum impact tester—Model Resil 50B (Ceast USA Inc. Charlotte, NC). Toughness was determined by integrating the area under the tensile stress vs. strain curve until the sample failed.

2.9 Statistical analysis

Statistical analysis was conducted using JMP® Software Version 16 (SAS Institute Inc., Cary, NC). Mechanical properties were analyzed using Tukey's Honestly Significant Difference (HSD) mean comparison of each group with the equation:

$$Y_{ijk} = A_i + B_j + C_k + \epsilon_{ijk}$$

where Y_{ijk} represents each mechanical property; the letters A , B , and C represent the fixed effect of each reinforcement at varying levels of wt.%; and ϵ term represents the error. This test was chosen as a conservative analysis of variance with respect to the unequal sample sizes between groups.

3 Results and discussion

3.1 Scanning electron microscopy

The SEM images at $\times 50$ magnification in Fig. 2 show a change in roughness in the PLA matrix with increased ESNF filler, specifically the 15 wt.% 4:1-nf (d) and 12 wt.% PVA-nf (g). However, a threshold exists where the increased roughness only occurred in composites with filler content above 4–6 wt.% ESNF filler, like that observed in 20 wt.% CNCs and poly(ethylene brassylate) composites [39]. In this study, the composite break surface roughness was attributed to the fiber distribution, the close proximity of fibers with hydroxyl (-OH) functionalities to the PLA matrix that promoted hydrogen bonding [40], and the increased complexity of stress transfers throughout the matrix that was attributed to the long fiber reinforcement. High magnification ($\geq 10 \text{ k}\times$) images of neat PLA and the composite test coupons are shown in Fig. 3 where evenly distributed fiber holes or exposed ends are visible on the fracture surface. Gavande et al. modeled ESNF nylon-reinforced epoxy resins and bridging mechanisms through fracture analysis. The authors attributed exfoliation, partial exfoliation, and complete exfoliation to the nanofiber matrix interfacial strength [41]. Partial exfoliation or the

separation of the fiber from the matrix resulted in pores with diameters exceeding the fiber diameters and the presence of exposed fibers, indicating weaker interfacial compatibility. In this study, exfoliation was most visible in the 3:2-nf PLA composite fracture surface, shown from this in Fig. 3c while some nanofiber ends were visible in 4:1-nf and PVA-nf PLA filled PLA. With an increase in ESNF content, the surface roughness of the fracture surface and frequency of holes or exposed fibers increased. Additionally, with the increased CNC content in the ESNFs, a variable morphology was observed in the fiber. Visible characteristics included a smooth surface break in the 4:1-nf and neat PVA nanofibers, while a rough surface was observed in the 3:2-nf.

3.2 Atomic force microscopy (AFM)

Images produced by AFM provided a means to qualitatively observe the material property changes generated by the interactions between PLA/PVA and PVA/CNC, as shown in Fig. 4. The topography, shown in Fig. 5a, c, and e, of the section of composite surface was produced from signal feedback within the closed loop (set point amplitude) from the sample z-piezo [42]. In the topographic images, the white represents the highest point ($\sim 40 \text{ nm}$) and the black the lowest point (-40 nm), with increased heights occurring by tip interactions with stiffer materials like cellulose in comparison to PLA. The AFM amplitude modulation technique simultaneously generates phase contrast imagery in a second output to sense qualitative material differences. These differences are produced from changes in the tip's deflection upon a brief interaction resulting from polymer viscoelastic properties, stiffness, and increased forces within the closed loop [43, 44].

The circular fiber morphologies observed in the height (black and white) are represented by the relative phase change and assigned an arbitrary color scale, shown in Fig. 4b, d, and f. The fiber cross-section dimensions, represented by blue, green, and yellow, are consistent in dimension with the sub-micrometer diameters observed in SEM images (Fig. 3a and b). However, variable surface roughness from cutting the neat PLA before observation with AFM, as shown in Fig. 4a, may not accurately represent the relative stiffness with respect to phase changes on the surface of the neat polymer because of the drastic height differences. Color changes in ESNF composites more strongly suggest material stiffness differences attributed to phase changes. The greater change in phase is attributed to the higher stiffness of the randomly oriented CNCs along the inside the ES fiber (blue) [45]. The phase change is less in the interphase region surrounding the CNCs or in ES fibers with a lower concentration of CNC ends within the cross section (green/yellow), and

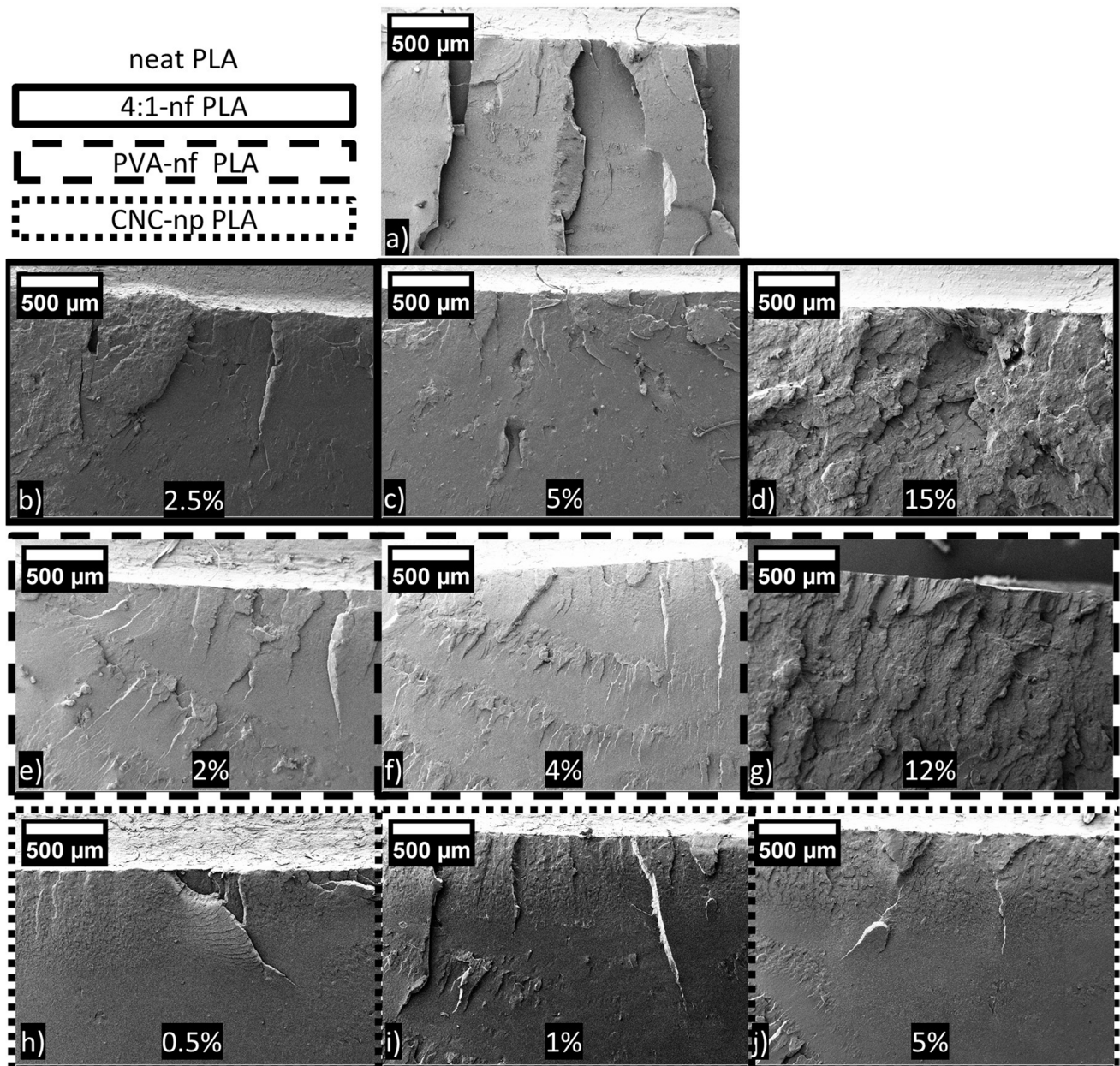


Fig. 2 SEM micrographs of each filler type (wt.%) PLA composite impact test specimen's break surface at $\times 50$ magnification

the lowest phase change is attributed to the matrix (yellow/brown). Further examination by force curve analysis or force modulation is needed to verify stiffness changes based on the initial phase contrast observations, but initial observations indicate that fiber surfaces are engaged with the matrix without voids forming near the fiber interface after cutting the specimen surface. A transcrystalline layer at the interface of the fiber and the PLA matrix may explain the phase change from green to yellow. The interactions of the -OH groups within the fiber and between the fiber and the matrix interface are observed via FTIR analysis.

3.3 FTIR

FTIR spectra were measured to qualify molecular interactions between the neat and composite ESNF filler and PLA matrix. The CNC-np was also measured for comparison. Intermolecular bonding of hydroxyl groups is indicated by the broad $3550\text{--}3200\text{ cm}^{-1}$ region. Rojas et al., in their characterization of composite ESNFs with PVA and CNC, reported two characteristic peaks that indicated free and bound -OH groups within this region [46]. In the spectra for this study, shown in Fig. 5, the former appeared around 3340 cm^{-1} and the latter around 3295 cm^{-1} . In observation of the fillers by type,

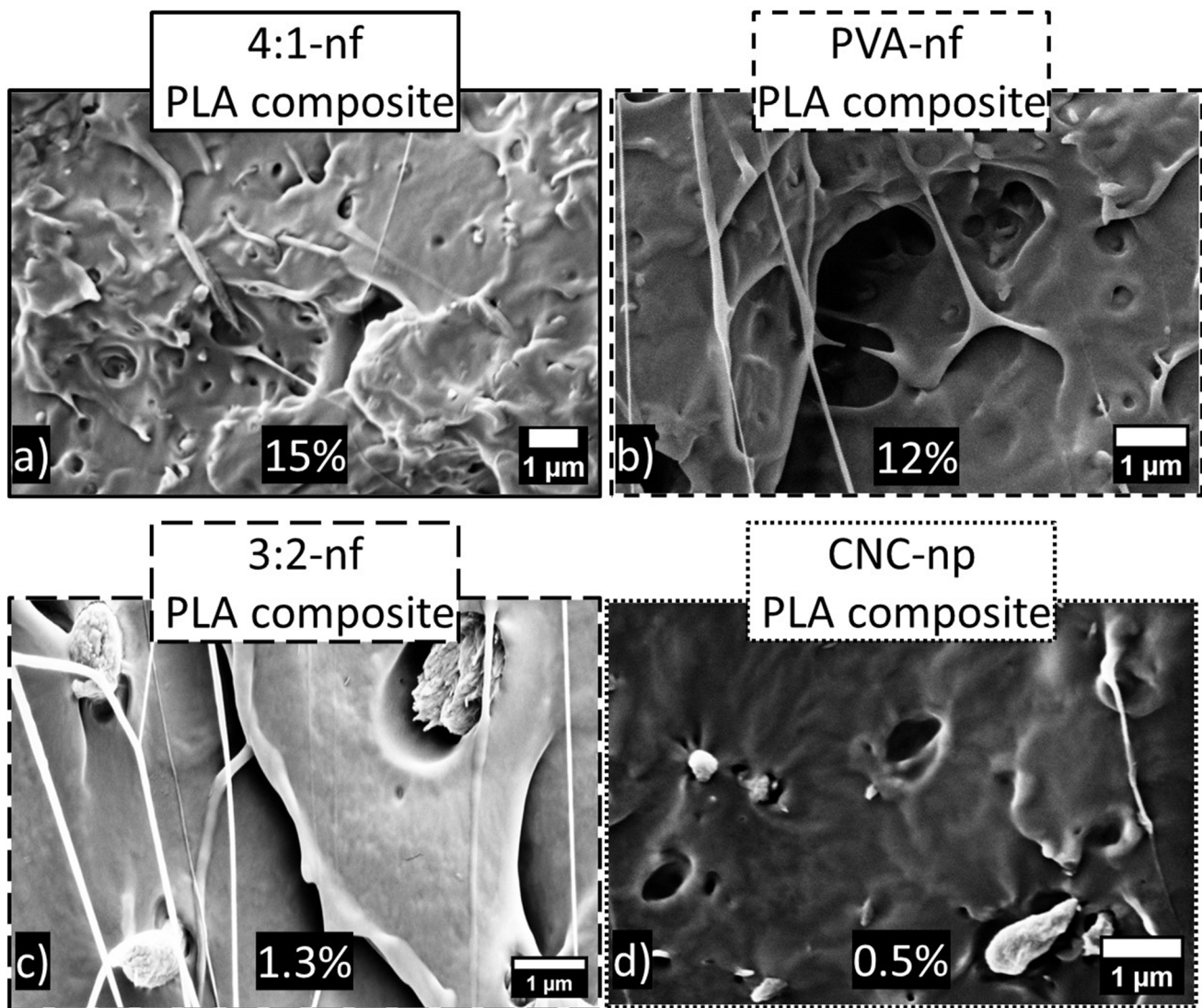


Fig. 3 SEM micrographs of ESNF-reinforced PLA impact test coupon break surfaces high magnification

shown in Fig. 5c, the free peak was most prominent in the CNC-np, and with increasing CNCs in the composite ESNFs, the free peak intensity shifted towards the bound wavenumber, appearing more like neat PVA-nf. The C-H stretching regions were observed between 2840 and 3000 cm^{-1} with PVA peaks (annotated with black text in Fig. 5C1) appearing at 2939, 2909, and 2863 cm^{-1} . The CNC peaks appeared at 2943, 2900, and 2854 cm^{-1} , and the composite ESNFs appeared in line with the PVA-nf frequencies.

In the composite ESNF-reinforced PLA, the peak intensity between 3200 and 3500 cm^{-1} increased with a large wt.% filler for both ratios and PVA-nf, which were relatively lower in the 3:2-nf filler (not shown). Further indications of -OH interactions (bending and stretching) were observed in the 1330–1420 and 1150–1000 cm^{-1} regions with peaks around 1080 cm^{-1} . Interactions between PVA and PLA

is reported to appear around 1750 and 1185 cm^{-1} by the carbonyl (C=O stretching) and the ester (C-O stretching) [47]. However, in the results shown in Fig. 5a and b, the respective peaks were observed at 1745 and 1180 cm^{-1} . A similar effect was observed in CNC-np filled PLA in Fig. 5c. Both the amorphous and α crystalline bands of PLA were visible at 955 cm^{-1} and 921 cm^{-1} , respectively, indicating that the crystallinity of PLA is somewhat affected by larger quantities of PVA-nf content, but this effect requires further investigation by differential scanning calorimetry (DSC) and X-ray diffraction (XRD) analysis.

3.4 Thermal properties

Thermal properties obtained by DSC analysis, shown in Table 3, include the glass transition (T_g) and melting (T_m)

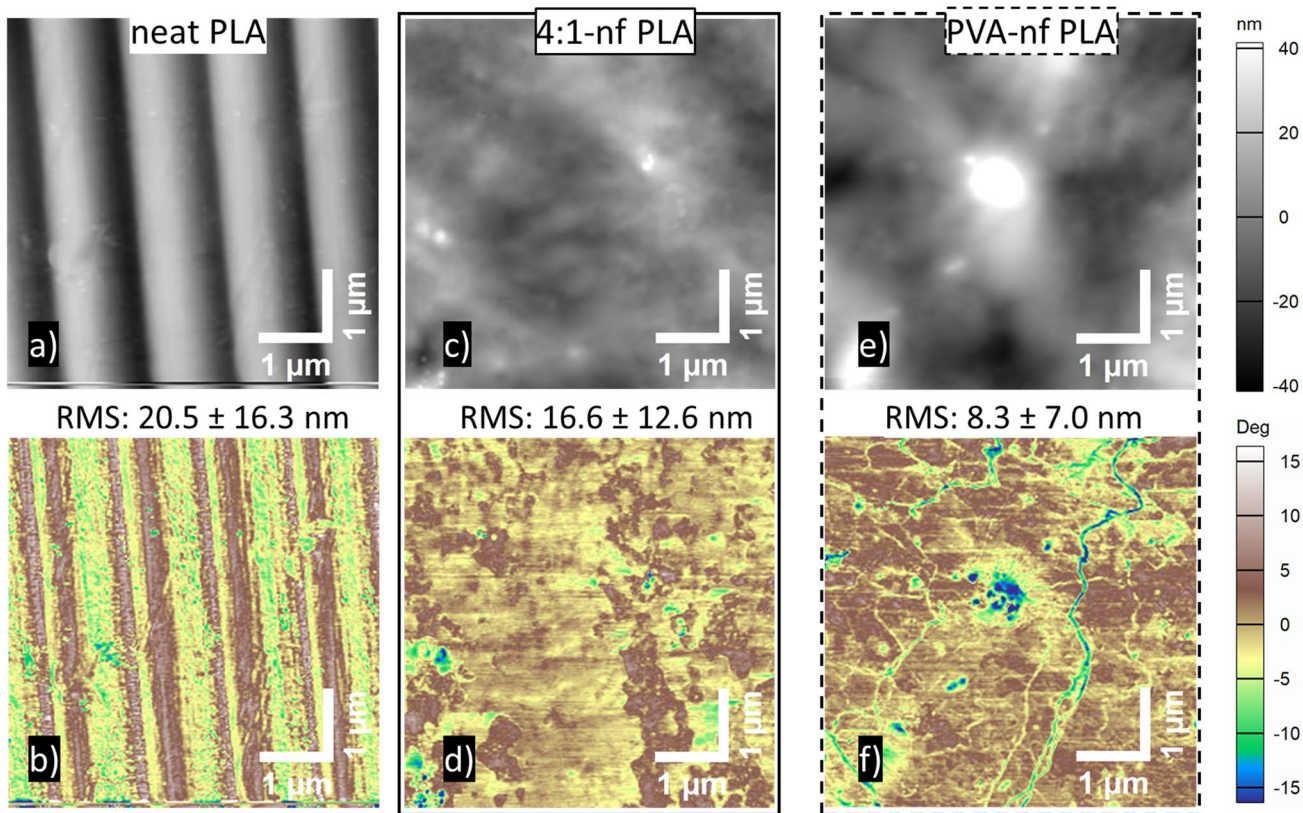


Fig. 4 Topographic (nm), phase contrast ($^{\circ}$), and surface roughness (nm) output in $5\text{-}\mu\text{m}^2$ cross sectional areas of neat PLA (a, b), PVA-nf PLA (c, d), and PVA:CNC-nf PLA (e, f); root mean square, RMS

Fig. 5 FTIR spectra of 4:1-nf (a), PVA-nf (b), and CNC-np filled PLA (c), including the fillers without matrix (d), broken into three sections: $3600\text{--}1200$ (a–d), 1300-- ($a_1\text{--}d_1$) and $980\text{--}900\text{ cm}^{-1}$ ($a_2\text{--}d_2$)

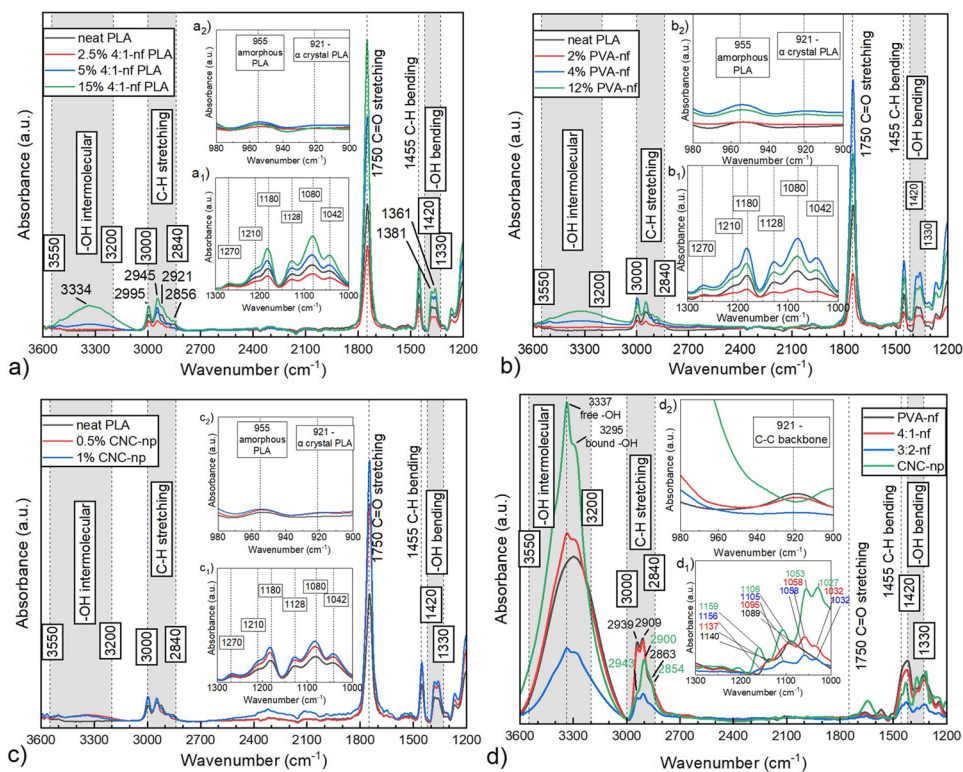


Table 3 Second heating cycle DSC and crystallinity percent calculation results of ESNF and CNC nano particle-reinforced composite PLA

ID	wt. (%)	T_g (°C)		T_m (°C)		H_{cc} (J/g)		H_m (J/g)		X_c (%)	
		μ	\pm	μ	\pm	μ	\pm	μ	\pm	μ	\pm
PLA	100	58.9	0.1	149.0	0.1	22.7	0.5	25.0	0.5	2.4	0.1
4:1-nf	2.5	58.6	0.1	149.2	0.3	20.9	1.9	22.2	1.1	1.3	0.9
	5	58.3	0.1	148.4	0.1	21.5	0.3	25.6	0.0	4.6	0.4
	15	57.4	0.3	153.2	0.2	23.5	0.4	26.1	0.4	3.2	0.3
	PVA-nf	2	59.1	0.4	149.9	0.7	20.8	1.5	23.9	0.9	3.4
PVA-nf	4	58.4	0.1	149.3	0.1	22.1	0.3	25.1	0.2	3.4	0.4
	12	57.9	0.5	148.5	0.9	23.3	1.3	26.0	0.2	3.3	1.5
	CNC-np	0.5	58.9	0.3	149.7	0.5	19.7	0.5	22.9	0.1	3.5
CNC-np	1	58.9	0.1	149.2	0.1	20.5	0.5	23.3	0.3	3.0	0.2
	3	58.7	0.2	149.0	0.4	19.4	0.0	21.5	0.1	2.4	0.1
	3:2-nf	1.3	58.7	0.2	149.1	0.2	22.0	0.5	25.2	0.2	3.5
3:2-nf	2.6	58.8	0.3	149.4	0.4	23.5	0.8	25.5	0.3	2.2	0.5
	7.5	57.3	0.4	148.8	3.3	23.8	0.6	25.9	0.4	2.4	0.9
	PVA2-nf	0.8	58.6	0.1	149.3	0.1	21.8	0.2	24.3	0.2	2.7
PVA2-nf	1.6	58.8	0.2	149.6	0.5	21.9	0.8	25.0	0.2	3.4	0.9
	4.5	58.2	0.1	148.0	0.1	26.2	0.1	27.8	0.1	1.8	0.2

temperatures (°C), enthalpy of cold crystallization (H_{cc}) and melting (H_m), and percentage of crystallinity (χ_c). Glass transition in the first heating cycle was a few degrees higher in each sample group (not listed) but reduced after annealing for 5 min at 200 °C. Addition of the ENSF did not appear to hinder PLA chain mobility with respect to a negligible change in T_g from PLA. Melting temperature also showed little change after the first heating cycle and annealing at 200 °C for 5 min, apart from the 15% 4:1-nf group, which showed a 4.2 °C increase. Despite previous studies, which indicated PVA up to 8% CNCs in composite films did not improve thermal resistance [17], the 4:1-nf at 15% (with 12% PVA and 3% CNCs) imparted some thermal resistance in PLA with the 153.2 ± 0.2 °C melting temperature in comparison with the 149 ± 0.1 °C PLA, which is currently not well understood and requires further investigation using thermogravimetric analysis. However, a secondary melt peak was observed in the PVA-nf 12% and 4:1-nf 15% groups DSC graph shown in Fig. 6 and suggests that the crystallization effect that is observed between PVA and CNCs, reported by Niinivaara et al. [48] studying thick films, affects the crystallinity in the PLA ESNF composite. Often, nucleation is detected by DSC analysis when measuring heat flow of composites containing small particles in semicrystalline polymer matrix [49]. An increase in crystallinity was observed to varying degrees and is listed in Table 3.

The PLA selected for this study is an amorphous grade and contains low crystallinity, reportedly from high D-lactide stereoisomer [50]. Addition of cellulose containing filler improved the X_c to 3.5% with 1.3 wt.% 3:2-nf, and with increased fiber content, it decreased to 2.2 and 2.4% X_c , which was consistent among most ESNF filled PLA.

However, thermal conductivity has been shown to improve in cellulose filled PVA ESNFs and could be attributed to a crystallization window at the 10 °C/min cooling rate used in this study [51]. Inconsistencies may be attributed to the distribution of fillers during melt mixing and potentially resolved by compounding in a twin-screw extrusion system.

3.5 Density

The calculated density was subtracted by the measured density, performed based on buoyancy (ASTM D792) that is listed in Table 4, and divided by the ideal density to give void fraction (V_f , %). Void content calculations were performed based on the weight fraction of the contents with respect to the theoretical volume based on the sum of constituent material density.

$$V_f = 100 * \frac{\rho_c - \rho_{exp}}{\rho_c}$$

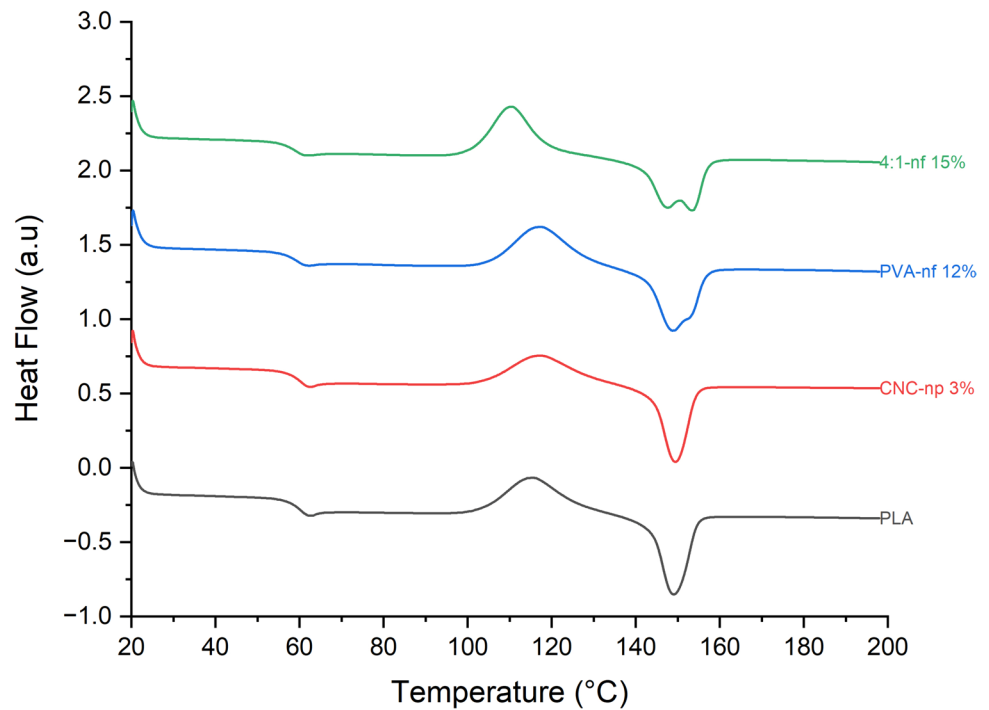
where ρ_c is the theoretical density and ρ_{exp} is the experimental density. The theoretical density was calculated using the equation

$$\frac{1}{\rho_c} = \sum_{i=1}^n \frac{W_i}{\rho_i}$$

where 1 is divided by the sum of the respective weight fraction of the components W_i divided by the constituent materials density ρ_i .

The void calculation results for all samples were negative values and may indicate the lack of accuracy in determining

Fig. 6 Graph of second DSC heating run of neat PLA and composite specimens



the experimental density of the composite. Additionally, improvements in the crystallinity of the composites were attributed to the change in experimental density which resulted in ostensibly void free composites. Literature regarding this subject notes that a 1% change in void calculation can occur with 1% error in the theoretical density [52]. It is well known that compounds containing small particles create nucleation in semicrystalline polymer matrices.

3.6 Mechanical properties

Melt compounded ESNFs generally improved the tensile yield strength (TYS) of PLA as shown in Fig. 7 with values listed in Table 5. The 2.5 wt.% composite 4:1-nf initially increased TYS by 17%, but with increased loading levels to 15 wt.%, the TYS improved 21% to 68.3 ± 1.2 MPa. In comparison, 3:2-nf improved tensile strength by 8 and 15% in the 1.3 and 2.6 wt.% groups, but by 3% with 7.5 wt.% filler in PLA. Previous work determined a 1:1 PVA:CNC fiber mat stiffness was $2.6 \times$ that of 4:1 ratio mat and may translate to the 3:2-nf [22]. Additionally, the 15% coefficient of variance (COV) in the 7.5 wt.% 3:2-nf was attributed to potential inconsistency in the fiber reinforcement performance, sample defects, or inconsistent distribution of fibers within the PLA matrix from less PVA content in the fiber. ESNFs may have also entangled into fiber bundles and remain undispersed during compounding; PLA composites containing neat PVA fillers, between both control groups, improved TYS 15–20%, from 64.9 ± 0.1 with 1.6 wt.% PVA2-nf and to 67.8 ± 1.8 with 4 wt.% PVA-nf.

Table 4 Calculated density with mean experimental density, standard deviation, and percentage difference from PLA

ID	wt (%)	ρ_c	$\mu \rho_{exp}$ (g/cm ³)	ρ_{exp} (\pm)	$\Delta \rho_{exp}$ (%)
PLA	0	1.240	1.251	0.004	0.00
4:1-nf	2.5	1.240	1.247	0.007	-0.32
	5	1.240	1.252	0.008	0.08
	15	1.240	1.269	0.013	1.44
PVA-nf	2	1.239	1.254	0.006	0.24
	4	1.238	1.247	0.003	-0.32
	12	1.234	1.252	0.007	0.08
CNC-np	0.5	1.241	1.245	0.006	-0.48
	1	1.241	1.268	0.003	1.36
	3	1.242	1.264	0.004	1.04
3:2-nf	1.3	1.246	1.253	0.002	0.16
	2.6	1.241	1.253	0.003	0.16
	7.5	1.244	1.258	0.007	0.56
PVA2-nf	0.8	1.240	1.244	0.012	-0.56
	1.6	1.239	1.250	0.008	-0.08
	4.5	1.238	1.260	0.007	0.72

The CNCs showed improvements in 3% and 5 wt.% specimens. Previous work, using a TSE to compound CNC-np at the same weight percentage showed a 10% improvement in strength [38].

Statistical analysis using Tukey's HSD mean comparison and letter difference among filler wt.% listed in Table 6 determined changes in TYS which were insignificant, apart

Fig. 7 Tensile yield strength (TYS, left) and tensile modulus of elasticity (TMOE, right) percentage change by filler (wt.%) and organized by filler type

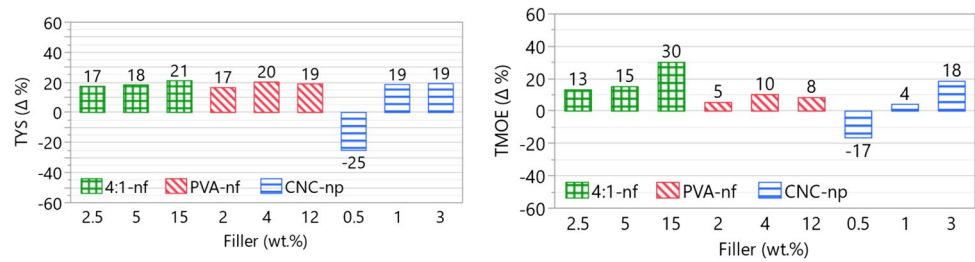


Table 5 Mean (μ) tensile and flexural properties of composite PLA groups including the standard deviations (\pm) and percent change (Δ ,%) by filler (wt.%)

Type ID	Filler wt.%	TYS (MPa)			TMOE (GPa)			TSb (%)			FYS (MPa)			FMOE (GPa)		
		μ	\pm	Δ %	μ	\pm	Δ %	μ	\pm	Δ %	μ	\pm	Δ %	μ	\pm	Δ %
PLA	100	56.4	13.6	0.0	3.64	0.76	0	2.6	1.5	0	99.6	6.4	0	3.68	0.09	0.0
4:1-nf	2.5	66.2	0.6	17.4	4.12	0.11	13.1	2.9	0.2	11.1	101.2	1.4	1.6	3.49	0.09	-5.2
	5	66.7	0.3	18.3	4.19	0.49	15.1	2.9	0.3	10.3	101	1.8	1.4	3.61	0.02	-1.9
	15	68.3	1.2	21.1	4.74	0.34	30.1	2.4	0.2	-7	100.4	0.6	0.8	3.91	0.21	6.3
PVA-nf	2	65.7	1.2	16.5	3.83	0.46	5.3	2.7	0.3	5.4	101.7	1.6	2.1	3.48	0.08	-5.4
	4	67.8	1.8	20.2	4.01	0.1	10.2	2.8	0.4	5.7	98.2	1.4	-1.4	3.41	0.02	-7.3
	12	67.1	0.9	19.0	3.94	0.31	8.3	3.2	0.3	23.5	99.4	1.9	-0.2	3.61	0.11	-1.9
CNC-np	0.5	42.2	10.9	-25.2	3.04	0.36	-16.5	2.0	0.5	-23.3	98.4	4.4	-1.2	3.07	0.14	-16.6
	1	66.9	0.3	18.6	3.79	0.32	4.2	2.1	1.2	10.3	106.7	0.6	7.1	3.66	0.09	-0.5
	3	67.2	0.4	19.1	4.31	0.32	18.4	2.7	0.1	-7	106.9	0.1	7.3	3.64	0.01	-1.1
3:2-nf	1.3	61.1	3.4	8.3	3.5	0.15	-4	2.4	0.3	-6.3	99.7	8.3	0.1	3.36	0.2	-8.7
	2.6	64.8	1.3	14.9	3.77	0.16	3.5	2.6	0.2	-1.4	104.9	3.9	5.3	3.47	0.01	-5.7
	7.5	57.9	9	2.7	4.04	0.45	11	2.0	0.4	-24.3	100.6	3.8	1.0	3.82	0.14	3.8
PVA2-nf	0.8	65.6	0.9	16.3	3.53	0.16	-3.1	2.8	0.2	8.7	107.6	1.1	8.0	3.47	0.1	-5.7
	1.6	64.9	0.1	15.1	3.78	0.4	3.8	2.8	0.1	8.1	96.3	7.1	-3.3	3.07	0.26	-16.6
	4.5	65.2	1.1	15.6	3.72	0.1	2.2	2.7	0.1	4.4	105.9	4.3	6.3	3.48	0.23	-5.4

from the 15 wt.% 4:1-nf. Strength improvements were attributed to interactions of hydroxyl groups in PVA with the ester bonds in thermoplastic PLA [47], as indicated by FTIR analysis shown in Fig. 5. The shift in unbound -OH groups improves the even distribution of the reinforcement fibers and increased the discontinuity in stress transfer across the sample. In effect, the surface roughness of broken samples from SEM images correlates with the statistical analysis letter difference of significant changes in TYS of the 15 wt.% 4:1-nf filler listed in Table 6. Figure 3a shows the even distribution of fibers and lack of fiber pull out that is attributed to the TYS improvement.

TYS tensile yield strength, TMOE tensile modulus of elasticity, TSb tensile strain at break, FYS flexural yield strength, FMOE flexural modulus of elasticity.

An apparent trend exists between 4:1-nf (wt.%) and tensile modulus of elasticity (TMOE) results, shown in Fig. 7 and listed in Table 5. Samples compounded with increasing wt.% of 4:1-nf showed increased TMOE of up to 4.74 ± 0.34 GPa, a 30% increase. PLA compounded with neat PVA-nf

increased at most 10.2% to 4.0 ± 0.1 GPa with 4 wt.% filler and reduced TMOE as little as 3.1% in 0.8 wt.% PVA2-nf. PLA composites containing 3:2-nf exhibited reduced TMOE at 1.3 wt.% and increased up to 11% to 4.04 ± 0.45 GPa with 2.6 wt.%. Statistical analysis attributed letter differences, listed in Table 6, was based on significance of mean comparisons among variations in filler wt.% in 4:1-nf and the CNC-np, but not among the neat PVA-nf and PVA2-nf or the 3:2-nf filled PLA groups. The observed improvements attributed to the 4:1-nf relate to the interfacial compatibility starting with the PVA encapsulated CNC fiber and translating to PVA shell interactions with the PLA matrix. Despite having more CNCs within the fiber, the 3:2-nf interacting with the PLA matrix, like the 4:1-nf, provided less intra fiber resistance to stress acting on the composite.

In support of this notion, Park et al. attributed hydrogen bonding and interaction of the ester linkages in the CNCs' anhydroglucose units with PVA hydroxyl groups (-OH) to the increased rigidity observed in the solvent cast films containing 3 and 5 wt.% CNCs [51]. Additionally, alignment of

Table 6 Statistical analysis on mechanical properties by Tukey's HSD mean comparison of filler types

Filler type	Filler (wt.%)	PLA (wt.%)	TYS	TMOE	FYS	FMOE	TSB	T	IS
4:1-nf	0	100	B	B	A	AB	A	B	B
	2.5	97.5	AB	AB	A	B	A	A	B
	5	95	AB	AB	A	B	A	AB	B
	15	85	A	A	A	A	A	AB	A
PVA-nf	0	100	A	A	A	A	A	B	AB
	2	98	A	A	A	A	A	AB	B
	4	96	A	A	A	A	A	A	AB
	12	88	A	A	A	A	A	A	A
CNC-np	0	100	A	AB	A	A	A	AB	A
	0.5	99.5	B	B	A	B	A	B	A
	1	99	A	AB	A	A	A	AB	A
	3	97	A	A	A	A	A	AB	A
3:2- nf	0	100	A	A	A	AB	A	A	B
	1.3	99.2	A	A	A	B	A	A	AB
	2.6	98.4	A	A	A	AB	A	A	AB
	7.5	95.5	A	A	A	A	A	A	A
PVA2-nf	0	100	A	A	A	A	A	A	B
	0.8	98.7	A	A	A	A	A	A	AB
	1.6	97.4	A	A	A	B	A	A	AB
	4.5	92.5	A	A	A	AB	A	A	A

CNCs was observed by solvent etching ESNF poly(methyl-methacrylate) (PMMA), observed with SEM, where Dong and co-workers concluded that alignment occurred during the polymer elongation phase (spinning) of sub-micron fiber formation [53]. In the same work, the author indicated that the fibers' modulus increased with the addition of CNCs up to 17 wt.%, as measured with nanoindentation, and that increased wt.% of CNCs were counterproductive to improving the elastic modulus. Moreover, Niinivaara et al. measured a 13-fold improvement in modulus with 10% CNCs that the author attributed to the CNCs forming a percolated network in thick PVA films, nucleating the PVA, and compatibility between the filler and matrix [48]. Considering the fiber content between the two ratios used in this study, the 4:1-nf falls within the increasing modulus effect, while the 3:2 ratio may distribute throughout the matrix; by reducing the PVA content available for surface interactions with PLA, the interfacial bond may provide less resistance to tensile stress during testing.

Tensile strain at break (TSB) of PLA increased when compounded with all wt.% of neat PVA-nf and at the lower wt.% of 4:1 ratio composite fiber; the values are listed in Table 5. Up to a 23.5% increase in strain was observed in 12 wt.% PVA-nf composite PLA, and less filler had a varied effect on TSB with improvements of 5–8% between PVA and PVA2-nf filled PLA. The 4:1-nf PLA composites showed improvements with 2.5 and 5 wt.% filler of 11.1 and 10.3%, respectively, but the 15 wt.% and all of the 3:2-nf reduced PLA TSB. Noteworthy, however, statistical analysis

determined that the TSB results of fiber and particle filled PLA composites were not significantly different from neat PLA by mean comparison (Table 6).

Flexural yield strength (FYS), illustrated in Fig. 8, exhibited $\pm 2\%$ changes when filled with ESNFs, apart from the 6–9% improvements observed in PVA2-nf. The filled materials within each ESNF type were not considered significantly different from neat PLA by statistical analysis, listed in Table 5. The CNC-np showed some increased FYS values, as cellulose nanomaterials in polymeric matrix are well known to improve flexural strength and stiffness [54, 55].

The addition of ESNFs generally produced a consistent reduction in flexural modulus of elasticity (FMOE), apart from the 6 and 4% increase observed in 15 wt.% 4:1-nf and 3:2-nf, respectively. The CNC-np showed a 1% reduction in FMOE, which is attributed to the low loading level (low volume) and short aspect ratio of CNCs [56]. Addition of CNCs was documented to reduce mechanical properties after reaching a percolation threshold [57].

3.6.1 Impact strength

Impact strength improvements, shown in Fig. 9, are typically attributed to the interfacial interaction of the fiber filler, the reduction in crack propagation, and increased complexity of stress transfer deviations in the matrix between the reinforcement fibers [58]. Williams et al. elaborate further, explaining that the key factors to controlling fracture energy relate to the fiber dimensions, mechanical

Fig. 8 Flexural yield strength (FYS, left) and flexural modulus of elasticity (FMOE, right) by filler (wt.%) and organized by filler type

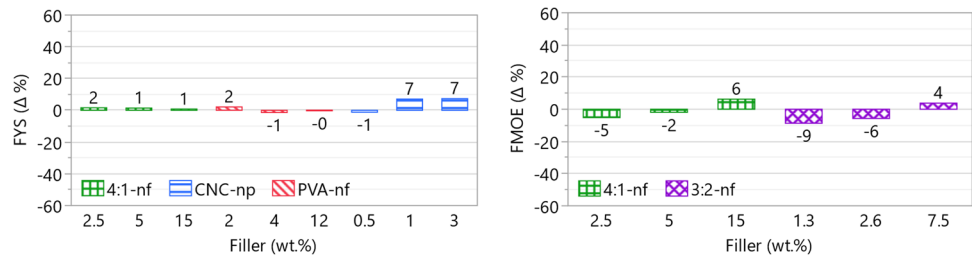
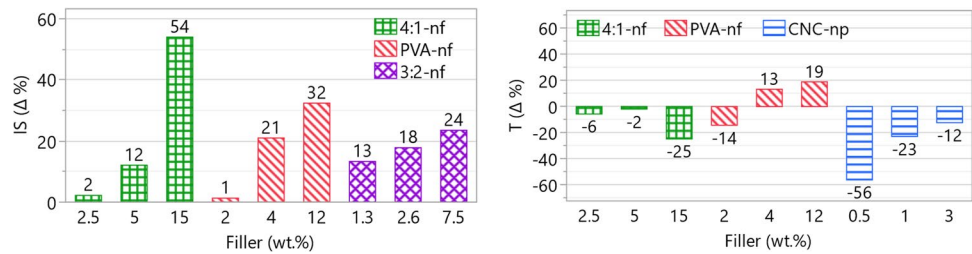


Fig. 9 Impact strength (IS, left) and modulus of toughness (T, right) by filler (wt.%) and organized by filler type



strength, volume fraction, and coefficient of friction during pull-out [59]. In this study, PLA compounded with PVA-nf and 4:1-nf improved the impact strength 32 and 54% with 12 and 15 wt.% ESNF reinforcement, listed in Table 7. The 7.5 wt.% PVA:CNC2-nf improved the IS of PLA by 23.5%, and the 4.5 wt.% PVA2-nf control showed a 27.6% improvement. The expectation of increasing impact strength with increasing PVA-nf in PLA was unsupported by the results of 2 and 4 wt.% sample groups. This implies an inconsistent dispersion of ESNFs among melt compounding of each formulation, presumably attributed to fiber agglomeration. In this study, statistical analysis of ESNF filled PLA by mean comparison of filler wt.% within

each filler type determined that all groups at the highest wt.% ESNFs were statistically significant from neat PLA. At lower levels, some overlap occurred, as indicated by letter differences that are shown in Table 6.

3.6.2 Toughness

Integration of the stress strain curves divided by density produced toughness (T, J/g) results [60]. The results are listed in Table 7 and illustrated in Fig. 9. The bar graph shows how composite ESNFs of both ratios, along with CNC-np, reduced the composite toughness, but the PVA-nf increased toughness by 19% with a 12 wt.% content in PLA.

Table 7 The mean (μ), toughness (T), and impact strength (IS) of composite PLA groups including the standard deviations (\pm) and percent change (Δ , %) by filler (wt.%) and type

Type ID	Filler wt.%	PVA:CNC w:w	IS (kJ/m ²)			T (J/g)		
			μ	\pm	$\Delta\%$	μ	\pm	$\Delta\%$
PLA	100	0:0	3.15	0.26	0	1.05	0.06	0.0
4:1-nf	2.5	4:1	3.22	0.30	2.2	0.99	0.18	-5.7
	5	4:1	3.53	0.70	12.1	1.03	0.13	-1.9
	15	4:1	4.85	0.86	54.0	0.79	0.04	-24.8
PVA-nf	2	1:0	3.19	0.38	1.3	0.9	0.1	-14.3
	4	1:0	3.81	1.00	21.0	1.19	0.15	13.3
	12	1:0	4.17	0.98	32.4	1.25	0.19	19.0
CNC-np	0.5	0:1	2.82	0.29	-10.5	0.46	0.26	-56.2
	1	0:1	3.20	0.30	1.6	0.81	0.25	-22.9
	3	0:1	3.35	0.62	6.3	0.92	0.03	-12.4
3:2-nf	1.3	3:2	3.57	0.06	13.3	0.71	0.18	-32.4
	2.6	3:2	3.71	0.36	17.8	0.85	0.11	-19.0
	7.5	3:2	3.89	0.63	23.5	0.51	0.23	-51.4
PVA2-nf	0.8	1:0	3.49	0.15	10.8	0.96	0.14	-8.6
	1.6	1:0	3.51	0.08	11.4	0.9	0.03	-14.3
	4.5	1:0	4.02	0.18	27.6	0.82	0.08	-21.9

Contrary to the 4 wt.% PVA-nf filler's 13% improvement to 1.19 ± 0.15 (J/g), the 4.5% PVA2-nf, as the control group for the 3:2 ratio composite, decreased the 1.05 ± 0.06 J/g PLA toughness by 21.9%, which would indicate poor mixing when compared to the former. Moreover, addition of CNC-np initially reduced the toughness by 56%; but with increasing levels, toughness decreased less by 12.4% and may indicate improved distribution with increased filler content. Liu and coworkers reported an increase in tensile yield strength with the addition of PVA in ESNF PLA mats but measured a decrease in toughness with 20 wt.% levels of PVA. A similar effect is observed in this study, where TYS values were improved in composite ESNF filled PLA, but the elongation decreased with increased filler amounts.

4 Discussion

4.1 Fiber effect and mechanical properties

In a review of natural fiber-reinforced composites [23], discussion surrounding aspect ratio expounds the effect of cellulose aspect ratio on the mechanical properties of a polymer matrix. Therein, small aspect ratio fibers improve the stiffness but reduce the strength from the fiber end effect [61], while high aspect ratio fibers improve both the strength and stiffness because of more surface interactions along the fibers length, an improved interfacial shear strength. The reduction of particle size to the nanoscale may contribute little to reinforcing a polymer matrix if the interfacial interactions with the matrix are poor. With increased surface interactions, the critical aspect ratio decreases, and smaller lengths are required for reinforcement. When compounding a polymer matrix with unsized CNC particles, the particles reportedly re-aggregate within the composite during extrusion [26]. With ESNF composites, the CNCs are encapsulated in the fiber before composite production. An added benefit of electrospinning is the increased specific surface area attributed to the nanoscale ESNF diameter. Compatibility between the polymer matrix and fiber is addressed via the material selection process, as opposed to a surface treatment or additive for chemical compatibility. Post processing ESNF mats by cutting fiber lengths of aligned mats allows for some consistency in the aspect ratio of cut fibers. This provides some consistency in the control of mechanical properties with respect to the fiber interfacial adhesion to the matrix and orientation parallel to the stressed axis [33, 62].

4.2 Surface characteristics and melt compounding

Colijn et al. notes that the polar and dispersive characteristics of the filler and polymer matrix should be similar for spontaneous mixing [27]. This applies to the PVA fiber and

PLA matrix and to the interaction of PVA and CNC during ES production of the composite nanofibers. The dispersive surface energy of PLA at 25 °C (298 K) was determined to be 33.3 mJ/m^2 [63]. Chen et al. determined that the dispersive energies of PVA, between 110 and 150 °C, were around 45 mJ/m^2 but could not extrapolate the value to room temperature [64]. Peng and Gardner measured dispersive energies of multiple varieties of commercial microcrystalline cellulose (MCC) and found the results ranged between 55 and 75 mJ/m^2 , depending on the manufacturing process [65]. Encapsulating the CNC in PVA may allow for more spontaneous mixing in molten PLA as the PVA coated CNCs are more closely related in surface energy compatibility, as opposed to CNCs self-affinity when compounded directly in PLA. Additionally, the PVA and CNC fiber specific strength improves with reduced dimensions, likely attributable to a closer proximity of fiber to matrix surface interaction [40], and offers the advantage of producing a hydrogen bonding network between each material in the composite.

4.3 ESNF composite fiber and PLA

The hydrogen bonding network, coupled with the high aspect ratio of the ESNFs, produced a noteworthy improvement in the toughness and impact properties in PLA composites containing PVA-nf and 4:1-nf, respectively. Control of the fiber lengths allows for greater utility of the mechanical properties imparted by the fiber [66]. In previous studies, elastomeric PLA blends greatly improved the strain at break and impact strength to $104 \pm 53.2\%$ and 59 ± 2.1 (kJ/m²) while reducing the tensile property performance [67]. Another study, that filled PLA with 20% acetyl tributyl citrate and 4 wt.% nano fibrillated cellulose (NFC), saw similar increases to elongation without as much tensile property loss [68]. By increasing the composite elongation and chain mobility, the tensile property performance cannot be maintained. However, coupling the ESNF reinforcement with a plasticizer and the use of long fibers with polymer specific surface interaction to provide interfacial compatibility could promote strength and stiffness improvements.

Over filling of CNCs in the 3:2-nf hindered the hydrogen bonding network between PVA and CNC, as indicated by FTIR (Fig. 5) and IS properties (Fig. 9), from performing as reinforcement on the level observed by the 4:1-nf reinforcement. Shalom et al. varied the ratios of CNC to PVA and encountered morphological changes that enhanced tensile strain and toughness in 1:5 PVA:CNC composite films by 570% and 202 MJ/m^3 , regardless of the crosslinker additive [19]. However, in this case, the improvements to toughness and strain failed to translate with thermally compounded PLA. One disadvantage in this study involved the small batch size in a bowl mixing unit. Between the PVA-nf and PVA2-nf filled PLA, mechanical property values were

inconsistent, which can be attributed to the distribution of fibers in the matrix. Adopting a masterbatch methodology was proven to increase dispersion of reinforcing agents in thermoplastics with a twin screw extrusion unit [69]. However, at the ESNF production levels used in this study, accumulating sufficient filler is prohibitively time consuming. However, high throughput techniques like free surface [70] or shear-aided [30] electrospinning could be utilized to address this setback.

5 Conclusions

Electrospun nanofibers were produced in quantities required to melt compound with PLA after mechanical cutting to a 1–5-mm length. The ESNFs were observed by SEM and AFM in the PLA matrix as partially exfoliated fibers protruding from the fracture surface after melt compounding. Long fiber length, nano-scale dimensions, and hydrogen bonding interactions were attributed to the tensile property improvements. A synergistic effect was observed by the 4:1 composite ESNF that lacked in the 3:2-nf PLA. The FTIR analysis indicated smaller peaks in the unbound -OH frequencies of ESNF fillers compared to CNC-np. At 15 wt.%, the 4:1-nf filled PLA exhibited the highest impact strength of improvement of a statistically significant 54%, maintained an increased T_m after 5 min of annealing at 200 °C, and reduced the tensile strain at break by 7% with a 21% and 30% improvement in tensile strength and modulus. The PVA-nf PLA exhibited improved strain at break and tensile strength by 19% and 24%, respectively. Furthermore, the toughness was improved in PVA-nf PLA composites. The flexural strength was statistically equal to neat PLA results with ESNF fillers. The bending modulus showed up to 6% and 4% improvement with 4:1 and 3:2 ratio composite ESNFs and decreased with all others by 5–10%. Table 8 summarizes the 4:1 ratio composite ESNF properties.

Acknowledgements The authors would like to thank the faculty and staff at the ASCC who helped to facilitate the completion of this work. Special thanks to the University of Maine's Electron Microscopy lab for AFM sample preparations with the microtome and operation of the Zeiss SEM.

Author contribution J. Elliott Sanders, Yousoo Han, Douglas J. Gardner contributed to the conception of the study. J. Elliott Sanders conducted electrospun fiber production, post-preparation, data collection, and analysis. Douglas J. Gardner, Yousoo Han, Todd S. Rushing, and Evan K. Wujcik provided testing methodology input and conceptual guidance in additional development of the research. J. Elliott Sanders wrote the first draft and compiled edits provided by all authors on previous drafts. All authors read and approved the final draft of the manuscript.

Funding This research was funded by the US Army Engineer Research Development Center (ERDC) under the grant entitled High Performance Materials and Structures (CS 20–0801 W52P1J-20–9-3014).

Table 8 Summarized mechanical property results with the mean (σ), standard deviation (\pm), and % change from neat PLA with 15 wt% 4:1 PVA:CNC-nf reinforcement

15 wt.% 4:1 PVA:CNC-nf results summary				
Property	Unit	μ	\pm	%
Tensile modulus of elasticity	GPa	4.74	0.34	30
Tensile yield strength	MPa	68.3	1.2	21
Tensile strain at break	%	2.4%	0.2%	–7
Flexural modulus of elasticity	GPa	3.91	0.21	6
Flexural yield strength	MPa	100.4	0.6	1
Impact strength	kJ/m ²	4.85	0.86	54

Data availability Raw data is available upon reasonable request and express third-party consent.

Declarations

Competing interests The author Dr. Evan Wujcik serves as editor for Advanced Composites and Hybrid Materials.

References

1. Abrha H et al (2022) Bio-based plastics production, impact and end of life: a literature review and content analysis. *Sustain* 14(8):1–20. <https://doi.org/10.3390/su14084855>
2. Liu Y et al (2020) Crystallization morphology regulation on enhancing heat resistance of polylactic acid. *Polymers (Basel)* 12(7):1–11. <https://doi.org/10.3390/polym12071563>
3. S. M. Ioannidou et al., “Techno-economic risk assessment, life cycle analysis and life cycle costing for poly(butylene succinate) and poly(lactic acid) production using renewable resources,” *Sci. Total Environ.*, vol. 806, 2022, <https://doi.org/10.1016/j.scitotenv.2021.150594>.
4. Mokhena TC, John MJ (Feb.2020) Cellulose nanomaterials: new generation materials for solving global issues. *Cellulose* 27(3):1149–1194. <https://doi.org/10.1007/s10570-019-02889-w>
5. Moon RJ, Schueneman GT, Simonsen J (2016) Overview of cellulose nanomaterials, their capabilities and applications. *Jom* 68(9):2383–2394. <https://doi.org/10.1007/s11837-016-2018-7>
6. Trache D, Hussin MH, Haafiz MKM, Thakur VK (2017) Recent progress in cellulose nanocrystals: sources and production. *Nanoscale* 9(5):1763–1786. <https://doi.org/10.1039/c6nr09494e>
7. Robles E, Urruzola I, Labidi J, Serrano L (2015) Surface-modified nano-cellulose as reinforcement in poly(lactic acid) to conform new composites. *Ind Crops Prod* 71:44–53. <https://doi.org/10.1016/j.indcrop.2015.03.075>
8. Zhang W, Zhang X, Liang M, Lu C (2008) Mechanochemical preparation of surface-acetylated cellulose powder to enhance mechanical properties of cellulose-filler-reinforced NR vulcanizates. *Compos Sci Technol* 68(12):2479–2484. <https://doi.org/10.1016/j.compscitech.2008.05.005>
9. Peng Y, Gardner DJ, Han Y (2012) Drying cellulose nanofibrils : in search of a suitable method. *Cellulose* 19:91–102. <https://doi.org/10.1007/s10570-011-9630-z>
10. Gardner DJ, Oporto GS, Mills R, Samir MASA (2008) Adhesion and surface issues in cellulose and nanocellulose. *J Adhes Sci*

- Technol 22(5–6):545–567. <https://doi.org/10.1163/156856108X295509>
11. Gardner D, Tajvidi M (2016) Hydrogen bonding in wood-based materials: an update. *Wood Fiber Sci* 48(4):234–244
 12. Faruk O, Bledzki AK, Fink HP, Sain M (2012) Biocomposites reinforced with natural fibers: 2000–2010. *Prog Polym Sci* 37(11):1552–1596. <https://doi.org/10.1016/j.progpolymsci.2012.04.003>
 13. Scaffaro R, Botta L, Lopresti F, Maio A, Sutura F (2017) Polysaccharide nanocrystals as fillers for PLA based nanocomposites. *Cellulose* 24(2):447–478. <https://doi.org/10.1007/s10570-016-1143-3>
 14. Gao Z, Peng J, Zhong T, Sun J, Wang X, Yue C (2012) Biocompatible elastomer of waterborne polyurethane based on castor oil and polyethylene glycol with cellulose nanocrystals. *Carbohydr Polym* 87(3):2068–2075. <https://doi.org/10.1016/j.carbpol.2011.10.027>
 15. Flieger M, Kantorová M, Prell A, Řezanka T, Votruba J (2003) Biodegradable plastics from renewable sources. *Folia Microbiol (Praha)* 48(1):27–44. <https://doi.org/10.1007/BF02931273>
 16. N. Ben Halima, “Poly(vinyl alcohol): review of its promising applications and insights into biodegradation,” *RSC Adv.*, vol. 6, no. 46, pp. 39823–39832, 2016, <https://doi.org/10.1039/c6ra05742j>.
 17. Rowe AA, Tajvidi M, Gardner DJ (2016) Thermal stability of cellulose nanomaterials and their composites with polyvinyl alcohol (PVA). *J Therm Anal Calorim* 126(3):1371–1386. <https://doi.org/10.1007/s10973-016-5791-1>
 18. M. Wang *et al.*, “Poly(vinyl alcohol) hydrogels: the old and new functional materials,” *Int. J. Polym. Sci.*, vol. 2021, 2021, <https://doi.org/10.1155/2021/2225426>.
 19. T. Ben Shalom *et al.*, “Cellulose nanocrystals (CNCs) induced crystallization of polyvinyl alcohol (PVA) super performing nanocomposite films,” *Macromol. Biosci.*, vol. 19, no. 3, 2019, <https://doi.org/10.1002/mabi.201800347>.
 20. Liu D, Li J, Sun F, Xiao R, Guo Y, Song J (2014) Liquid crystal microphase separation of cellulose nanocrystals in wet-spun PVA composite fibers. *RSC Adv* 4(58):30784–30789. <https://doi.org/10.1039/c4ra04063e>
 21. Yao L, Haas TW, Guiseppi-Elie A, Bowlin GL, Simpson DG, Wnek GE (2003) Electrospinning and stabilization of fully hydrolyzed poly(vinyl alcohol) fibers. *Chem Mater* 15(9):1860–1864. <https://doi.org/10.1021/cm0210795>
 22. J. E. Sanders, Y. Han, T. S. Rushing, and D. J. Gardner, “Electrospinning of cellulose nanocrystal-filled poly(vinyl alcohol) solutions: material property assessment,” *Nanomaterials*, vol. 9, no. 5, May 2019, <https://doi.org/10.3390/nano9050805>.
 23. J. Wang, L. Wang, D. J. Gardner, S. M. Shaler, and Z. Cai, *Towards a cellulose-based society: opportunities and challenges*, vol. 28, no. 8. Springer Netherlands, 2021. <https://doi.org/10.1007/s10570-021-03771-4>.
 24. B. J. Holland and J. N. Hay, “The thermal degradation of poly(vinyl alcohol),” vol. 42, pp. 6775–6783, 2001.
 25. Peng Y, Gardner DJ, Han Y, Kiziltas A, Cai Z, Tshabalala MA (2013) Influence of drying method on the material properties of nanocellulose I: thermostability and crystallinity. *Cellul* 20(5):2379–2392. <https://doi.org/10.1007/s10570-013-0019-z>
 26. Bondeson D, Oksman K (2007) Polylactic acid/cellulose whisker nanocomposites modified by polyvinyl alcohol. *Compos Part A Appl Sci Manuf* 38(12):2486–2492. <https://doi.org/10.1016/j.compositesa.2007.08.001>
 27. Colijn I, Schroën K (2021) Thermoplastic bio-nanocomposites: from measurement of fundamental properties to practical application. *Adv Colloid Interface Sci* 292:102419. <https://doi.org/10.1016/j.cis.2021.102419>
 28. D. H. Reneker, A. L. Yarin, H. Fong, and S. Koombhongse, “Bending instability of electrically charged liquid jets of polymer solutions in electrospinning,” *J. Appl. Phys.*, vol. 87, no. 9 I, pp. 4531–4547, 2000, <https://doi.org/10.1063/1.373532>.
 29. H. Niu and T. Lin, “Fiber generators in needleless electrospinning,” *J. Nanomater.*, vol. 2012, 2012.
 30. Kara Y, He H, Molnár K (Oct.2019) Shear-aided high-throughput electrospinning: a needleless method with enhanced jet formation. *J Appl Polym Sci* 137(37):49104. <https://doi.org/10.1002/app.49104>
 31. Thoppey NM, Bochinski JR, Clarke LI, Gorga RE (Aug.2011) Edge electrospinning for high throughput production of quality nanofibers. *Nanotechnology* 22(34):345301. <https://doi.org/10.1088/0957-4484/22/34/345301>
 32. Jiang S *et al* (2018) Electrospun nanofiber reinforced composites: a review. *Polym Chem* 9(20):2685–2720. <https://doi.org/10.1039/c8py00378e>
 33. Baji A, Mai YW, Wong SC, Abtahi M, Chen P (2010) Electrospinning of polymer nanofibers: effects on oriented morphology, structures and tensile properties. *Compos Sci Technol* 70(5):703–718. <https://doi.org/10.1016/j.compscitech.2010.01.010>
 34. Wang G, Yu D, Kelkar AD, Zhang L (2017) Electrospun nanofiber: emerging reinforcing filler in polymer matrix composite materials. *Prog Polym Sci* 75:73–107. <https://doi.org/10.1016/j.progpolymsci.2017.08.002>
 35. Toriello M, Afsari M, Shon HK, Tijing LD (2020) Progress on the fabrication and application of electrospun nanofiber composites. *Membranes (Basel)* 10(9):1–35. <https://doi.org/10.3390/membranes10090204>
 36. Zhang X, Shi X, Gautrot JE, Peijs T (Jan.2021) Nanoengineered electrospun fibers and their biomedical applications: a review. *Nanocomposites* 7(1):1–34. <https://doi.org/10.1080/20550324.2020.1857121>
 37. Shakil UA, Hassan SBA, Yahya MY, Nauman S (2020) Mechanical properties of electrospun nanofiber reinforced/interleaved epoxy matrix composites—a review. *Polym Compos* 41(6):2288–2315. <https://doi.org/10.1002/pc.25539>
 38. Sanders JE, Wang L, Brinkley G, Gardner DJ (2023) Production of nano-scale cellulose nanocrystal powder via electrospray drying (ESD) for sustainable composites. *Cellulose*. <https://doi.org/10.1007/s10570-023-05217-5>
 39. Butron A, Llorente O, Fernandez J, Meaurio E, Sarasua JR (2019) Morphology and mechanical properties of poly(ethylene brassylate)/cellulose nanocrystal composites. *Carbohydr Polym* 221(Febuary):137–145. <https://doi.org/10.1016/j.carbpol.2019.05.091>
 40. Wohler M, Benselfelt T, Wågberg L, Furó I, Berglund LA, Wohler J (2022) Cellulose and the role of hydrogen bonds: not in charge of everything. *Cellulose* 29(1):1–23. <https://doi.org/10.1007/s10570-021-04325-4>
 41. V. Gavande, S. Nagappan, B. Seo, Y. S. Cho, and W. K. Lee, “Transparent nylon 6 nanofibers-reinforced epoxy matrix composites with superior mechanical and thermal properties,” *Polym. Test.*, vol. 122, no. January, p. 108002, 2023, <https://doi.org/10.1016/j.polymertesting.2023.108002>.
 42. Scott WW, Bhushan B (2003) Use of phase imaging in atomic force microscopy for measurement of viscoelastic contrast in polymer nanocomposites and molecularly thick lubricant films. *Ultramicroscopy* 97(1–4):151–169. [https://doi.org/10.1016/S0304-3991\(03\)00040-8](https://doi.org/10.1016/S0304-3991(03)00040-8)
 43. Tamayo J, García R (1996) Deformation, contact time, and phase contrast in tapping mode scanning force microscopy. *Langmuir* 12(18):4430–4435. <https://doi.org/10.1021/la960189l>
 44. Raghavan D, Gu X, Nguyen T, VanLandingham M, Karim A (Apr.2000) Mapping polymer heterogeneity using atomic force

- microscopy phase imaging and nanoscale indentation. *Macromolecules* 33(7):2573–2583. <https://doi.org/10.1021/ma991206r>
45. Santos NDWRPO, Eichhorn CDEFSJ (2016) Orientation of cellulose nanocrystals in electrospun polymer fibres. *J Matr Sci* 51(1):218–227. <https://doi.org/10.1007/s10853-015-9409-y>
 46. Habibi Y, Zoppe JO, Rojas OJ, Peresin MS, Pawlak JJ (2010) Nanofiber composites of polyvinyl alcohol and cellulose nanocrystals: manufacture and characterization. *Biomacromol* 11(3):674–681. <https://doi.org/10.1021/bm901254n>
 47. Y. Liu, H. Wei, Z. Wang, Q. Li, and N. Tian, “Simultaneous enhancement of strength and toughness of PLA induced by miscibility variation with PVA,” *Polymers (Basel)*, vol. 10, no. 10, 2018, <https://doi.org/10.3390/polym10101178>.
 48. Niinivaara E, Desmaisons J, Dufresne A, Bras J, Cranston ED (2021) Thick polyvinyl alcohol films reinforced with cellulose nanocrystals for coating applications. *ACS Appl Nano Mater* 4(8):8015–8025. <https://doi.org/10.1021/acsnm.1c01244>
 49. Gray DG (2008) Transcrystallization of polypropylene at cellulose nanocrystal surfaces. *Cellulose* 15(2):297–301. <https://doi.org/10.1007/s10570-007-9176-2>
 50. M. A. Orteni *et al.*, “Synthesis of polylactic acid initiated through biobased antioxidants: towards intrinsically active food packaging,” *Polymers (Basel)*, vol. 12, no. 5, 2020, <https://doi.org/10.3390/POLYM12051183>.
 51. Y. Park *et al.*, “Thermal conductivity enhancement in electrospun poly(vinyl alcohol) and poly(vinyl alcohol)/cellulose nanocrystal composite nanofibers,” *Sci. Rep.*, vol. 9, no. 1, 2019, <https://doi.org/10.1038/s41598-019-39825-8>.
 52. Thomason JL (1995) The interface region in glass fibre-reinforced epoxy resin composites: 3. Characterization of fibre surface coatings and the interphase. *Composites* 26(7):487–498. [https://doi.org/10.1016/0010-4361\(95\)96806-H](https://doi.org/10.1016/0010-4361(95)96806-H)
 53. Dong H, Strawhecker KE, Snyder JF, Orlicki JA, Reiner RS, Rudie AW (2012) Cellulose nanocrystals as a reinforcing material for electrospun poly(methyl methacrylate) fibers: formation, properties and nanomechanical characterization. *Carbohydr Polym* 87(4):2488–2495. <https://doi.org/10.1016/j.carbpol.2011.11.015>
 54. Jonoobi M, Harun J, Mathew AP, Oksman K (2010) Mechanical properties of cellulose nanofiber (CNF) reinforced polylactic acid (PLA) prepared by twin screw extrusion. *Compos Sci Technol* 70(12):1742–1747. <https://doi.org/10.1016/j.compscitech.2010.07.005>
 55. Aitomäki Y, Oksman K (2014) Reinforcing efficiency of nanocellulose in polymers. *React Funct Polym* 85:151–156. <https://doi.org/10.1016/j.reactfunctpolym.2014.08.010>
 56. H. Kargarzadeh *et al.*, “Recent developments on nanocellulose reinforced polymer nanocomposites: a review,” *Polymer*, vol. 132. Elsevier Ltd, pp. 368–393, Dec. 06, 2017. <https://doi.org/10.1016/j.polymer.2017.09.043>.
 57. T. C. Mokhena, J. S. Sefadi, E. R. Sadiku, M. J. John, M. J. Mochane, and A. Mtibe, “Thermoplastic processing of PLA/cellulose nanomaterials composites,” *Polymers (Basel)*, vol. 10, no. 12, 2018, <https://doi.org/10.3390/polym10121363>.
 58. Mowade TK, Dange SP, Thakre MB, Kamble VD (2012) Effect of fiber reinforcement on impact strength of heat polymerized polymethyl methacrylate denture base resin: in vitro study and SEM analysis. *J Adv Prosthodont* 4(1):30–36. <https://doi.org/10.4047/jap.2012.4.1.30>
 59. Williams T, Allen G, Kaufman MS (1973) The impact strength of fibre composites. *J Mater Sci* 8(12):1765–1787. <https://doi.org/10.1007/BF02403530>
 60. Coleman JN *et al* (2004) High-performance nanotube-reinforced plastics: understanding the mechanism of strength increase. *Adv Funct Mater* 14(8):791–798. <https://doi.org/10.1002/adfm.200305200>
 61. N. Pan, “Exploring the significance of structural hierarchy in material systems - a review,” *Appl. Phys. Rev.*, vol. 1, no. 2, 2014, <https://doi.org/10.1063/1.4871365>.
 62. H. Yu, H. Zhang, M. Song, Y. Zhou, J. Yao, and Q. Ni, “From cellulose nanospheres, nanorods to nano fibers: various aspect ratio induced nucleation / reinforcing effects on polylactic acid for robust-barrier food packaging,” 2017, <https://doi.org/10.1021/acsami.7b09102>.
 63. Cava D, Gavara R, Lagarón JM, Voelkel A (2007) Surface characterization of poly(lactic acid) and polycaprolactone by inverse gas chromatography. *J Chromatogr A* 1148(1):86–91. <https://doi.org/10.1016/j.chroma.2007.02.110>
 64. S. Chen *et al.*, “Quantitative study on solubility parameters and related thermodynamic parameters of pva with different alcoholysis degrees,” *Polymers (Basel)*, vol. 13, no. 21, 2021, <https://doi.org/10.3390/polym13213778>.
 65. Peng Y, Gardner DJ (2015) Surface energy of cellulosic materials: the effect of particle morphology, particle size, and hydroxyl number. *TAPPI J* 14(9):565–576
 66. Ning H, Lu N, Hassen AA, Chawla K, Selim M, Pillay S (2020) A review of long fibre thermoplastic (LFT) composites. *Int Mater Rev* 65(3):164–188. <https://doi.org/10.1080/09506608.2019.1585004>
 67. N. Likittanaprasong, M. Seadan, and S. Suttiruengwong, “Impact property enhancement of poly(lactic acid) with different flexible copolymers,” *IOP Conf. Ser. Mater. Sci. Eng.*, vol. 87, no. 1, 2015, <https://doi.org/10.1088/1757-899X/87/1/012069>.
 68. J. Tian *et al.*, “Improving tensile strength and impact toughness of plasticized poly(lactic acid) biocomposites by incorporating nanofibrillated cellulose,” vol. 11, no. 1, pp. 2469–2482, 2022, <https://doi.org/10.1515/ntrev-2022-0142>.
 69. S. Boran, A. Kiziltas, E. E. Kiziltas, and D. J. Gardner, “The comparative study of different mixing methods for microcrystalline cellulose/polyethylene composites,” vol. 31, no. 1, pp. 92–103, 2016, <https://doi.org/10.3139/217.3156>.
 70. Jiang G, Zhang S, Wang Y, Qin X (2015) An improved free surface electrospinning with micro-bubble solution system for massive production of nanofibers. *Mater Lett* 144:22–25. <https://doi.org/10.1016/j.matlet.2014.12.139>

Publisher's Note Springer Nature remains neutral with regard to jurisdictional claims in published maps and institutional affiliations.

Springer Nature or its licensor (e.g. a society or other partner) holds exclusive rights to this article under a publishing agreement with the author(s) or other rightsholder(s); author self-archiving of the accepted manuscript version of this article is solely governed by the terms of such publishing agreement and applicable law.